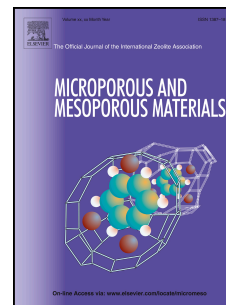# Accepted Manuscript

Hybrid materials based on polyethylene and MCM-41 microparticles functionalized with silanes: Catalytic aspects of in situ polymerization, crystalline features and mechanical properties

M.L. Cerrada, A. Bento, E. Pérez, V. Lorenzo, J.P. Lourenço, M.R. Ribeiro

Please cite this article as: M.L. Cerrada, A. Bento, E. Pérez, V. Lorenzo, J.P. Lourenço, M.R. Ribeiro, Hybrid materials based on polyethylene and MCM-41 microparticles functionalized with silanes: Catalytic aspects of in situ polymerization, crystalline features and mechanical properties, *Microporous and Mesoporous Materials* (2016), doi: 10.1016/j.micromeso.2016.06.011.

This is a PDF file of an unedited manuscript that has been accepted for publication. As a service to our customers we are providing this early version of the manuscript. The manuscript will undergo copyediting, typesetting, and review of the resulting proof before it is published in its final form. Please note that during the production process errors may be discovered which could affect the content, and all legal disclaimers that apply to the journal pertain.
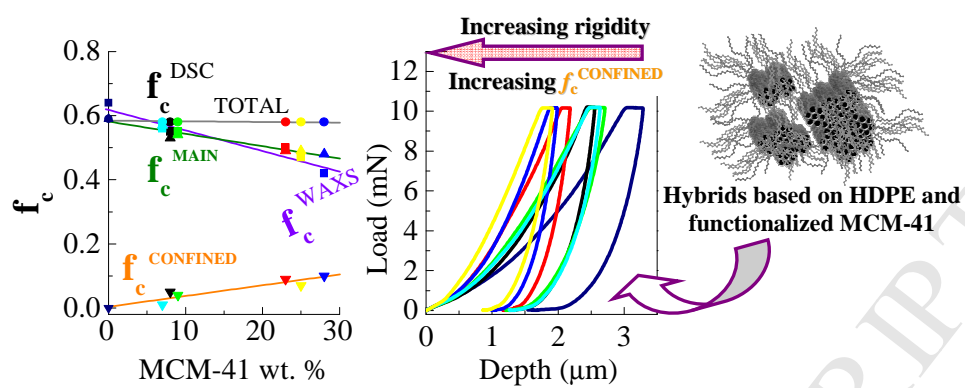
Hybrid Materials Based on Polyethylene and MCM-41 Microparticles Functionalized with Silanes: Catalytic Aspects of In Situ Polymerization, Crystalline Features and Mechanical Properties

M. L. Cerrada*[a], A. Bento[b], E. Pérez[a], V. Lorenzo[c], J. P. Lourenço[d,b], M. R. Ribeiro*[b]

[a]Instituto de Ciencia y Tecnología de Polímeros (ICTP-CSIC). Juan de la Cierva 3, 28006 Madrid, Spain.

[b]Centro de Química Estrutural (CQE) & Instituto Superior Técnico, Universidade de Lisboa. Av. Rovisco Pais, 1049-001 Lisboa, Portugal.

[c]Grupo de Investigación ''POLímeros: Caracterización y Aplicaciones" (U. A. del ICTP-CSIC), E.T.S.I. Industriales, Universidad Politécnica de Madrid, José Gutiérrez Abascal 2, 28006 Madrid, Spain.

[d]Centro de Investigação em Química do Algarve (CIQA). Faculdade de Ciências e Tecnologia, Universidade do Algarve. Campus de Gambelas, 8005-139 Faro, Portugal.

*Corresponding authors.

Tel.: +34-915622900; Fax: +34-915644853; E-mail address: mlcerrada@ictp.csic.es

Tel.: +351-218417325; Fax: +351-218419198; E-mail address: rosario@tecnico.ulisboa.pt

Abstract

New nanocomposites based on polyethylene have been prepared by in situ polymerization of ethylene in presence of mesoporous MCM-41. The polymerization reactions were performed using a zirconocene catalyst either under homogenous conditions or supported onto mesoporous MCM-41 particles, which are synthesized and decorated post-synthesis with two silanes before polymerization in order to promote an enhanced interfacial adhesion. The existence of polyethylene chains able to crystallize within the mesoporous channels in the resulting nanocomposites is figured out from the small endothermic process, located at around 80 ºC, on heating calorimetric experiments, in addition to the main melting endotherm. These results indicate that polyethylene macrochains can grow up during polymerization either outside or inside the MCM-41 channels, these keeping their regular hexagonal arrangements. Mechanical response is observed to be dependent on the content in mesoporous MCM-41 and on the crystalline features of polyethylene. Accordingly, stiffness increases and deformability decreases in the nanocomposites as much as MCM-41 content is enlarged and polyethylene amount within channels is raised. Ultimate mechanical performance improves with MCM-41 incorporation without varying the final processing temperature.

*Keywords***:** Polyethylene; MCM-41 microparticles; silane; hybrids; crystallinity; rigidity.

1. **Introduction**

Interest on polymeric-based nanocomposites has exponentially grown up in the last decade and it is currently an area of extreme activity in order to develop new materials. Examples in literature exhibit significant improvements in mechanical, electrical, biocidal and thermal properties [1-7], which are difficult to be achieved using conventional fillers [8,9]. An aspect of significant impact, mainly in weight and cost, is the low reinforcement loadings required (typically inferior to 8 wt.%) to attain a noteworthy enhancement in properties. The key that triggers these low contents strongly depends on a suitable nanofiller–matrix interfacial adhesion that involves an optimal dispersion of nanofillers and their intimate contact with the polymeric matrix. Therefore, the formation of large size aggregates should be conveniently avoided.

Polyolefins comprise the most important thermoplastic polymers, owing to their low manufacturing cost and rather versatile properties. Then, polyolefins represent almost two-thirds of the major commodity thermoplastics used and have an impact on every daily life, in applications ranging from automotive parts to high modulus fibers, household and food containers, toys, stretch film/shrink film, highly sophisticated capacitor films, diapers and trash bags among others. Their applicability might be further spread out although new developments should be endowed to make polyolefins capable of competing with more specific and expensive polymers. Nanotechnology has become a valuable tool to improve their final properties, allowing obtainment of new functionalities and tunable responses for their use in advanced applications at affordable costs.

Ordered mesoporous silicas, with high surface area and pore sizes, have shown high potential as supports in olefin polymerization in recent years. For instance, metallocene catalysts supported on MCM-41 give rise to catalytic systems with interesting properties in terms of activity and polymer characteristics, due to the confinement effects that may arise from the polymerization inside the porous structure [10-12]. The polymerization of olefins using MCM-41-supported metallocene catalysts has also opened an interesting approach to prepare in situ (nano)composites, since MCM-41 shows a stable 3D framework that consists of hexagonal

arrangements with nanosized pores. This ordered structure confers to MCM-41 a high porosity and surface area [13] that makes possible in-situ polymerization of organic monomers within its pores. Furthermore, the existence of polymeric chains coming out from the channels might also favor interactions between the mesoporous silica and the polymer matrix that, as aforementioned, are critical to get materials with enhanced performance. Thus, improved mechanical properties [14] and an easier degradability [15] have been reported in hybrid materials prepared by in-situ ethylene polymerization in presence of MCM-41. Those mesoporous particles acted as catalyst supports and as inorganic fillers.

A recent step forward involved the use of undecenoic acid as an interfacial agent to provoke a reduction in effective aggregate size, attempting to hinder MCM-41 particle agglomeration and, consequently, to promote better MCM-41 particle dispersion. Those new materials showed an interesting gas permeation behavior [16] and an enhanced mechanical response [17] compared with those exhibited by their neat counterparts. Nevertheless, incorporation of undecenoic acid within the macromolecular architecture (even at a very small amount) implies a reduction in the polymeric crystallinity and crystal size. To overcome this shortcoming, organosilanes are now proposed to boost adhesion at organic-inorganic interfaces, since these molecules can be easily grafted onto the surface of silica MCM-41 via hydrolysis with superficial silanol groups. Stable covalent bonds can be formed and an important hydrophobic character may be created at the silica particle surface depending on the silane functionalities. This increase in the hydrophobicity of the silica particles could help to disperse them conveniently into the polymeric matrix. Recently, various organosilanes have been used as coupling agents [18] during preparation, by melt blending method, of silica/PP composites.

The main aim of this work is, therefore, the preparation of nanocomposites based on silane functionalized MCM-41 particles and high density polyethylene (HDPE) by in situ polymerization, as well as evaluation of their crystalline structure, thermal properties and mechanical behavior. To reach those purposes, the previous decoration of mesoporous MCM-41 particles with two different silanes, chloro(dimethyl)vinylsilane and trimethoxy(7-octen-1-yl)silane, is required for their use either only as fillers (polymerization taking place in a

3

homogeneous medium) or as catalyst supports and fillers (polymerization being carried out now under heterogeneous conditions). The effect of MCM-41 functionalization on the catalytic activity is analyzed in terms of the type of silane and of the polymerization approach used (homogeneous vs. heterogeneous). Once the materials are obtained, X-ray scattering measurements at wide and middle angle regions (WAXS and MAXS, respectively), differential scanning calorimetry (DSC) experiments, and scanning and transmission electron microscopy (SEM and TEM, respectively) observations have been carried out to evaluate the crystalline structure and morphological characteristics. Moreover, thermogravimetric measurements are used to examine their thermal stability. As well the viscoelastic and mechanical behavior of these materials is studied by performing dynamic mechanical thermal analysis (DMTA) tests and depth sensing indentation, DSI, experiments.

2. Experimental Section

2.1. Materials and Chemicals

All manipulations were performed under dry nitrogen using standard Schlenk techniques. Ethylene and nitrogen (Air Liquide) were purified through absorption columns containing molecular sieves 4A and 13X. Methylaluminoxane (MAO, 10 wt.% in toluene solution, Albermale), Cp_2ZrCl_2, chloro(dimethyl)vinylsilane (VS), trimethoxy(7-octen-1-yl)silane (OES), purchased from Aldrich were used as received. Toluene (Petrogal) was distilled over sodium under a dry nitrogen atmosphere, using benzophenone as indicator.

2.2. Preparation of MCM-41 particles

The synthesis procedure and the characterization of microsized MCM-41 particles are described extensively elsewhere [19], its structural parameters being reported in Table 1. MCM-41 was dried for 2h at 300 ºC with nitrogen purging, cooled and stored under dry nitrogen before its use.

2.3. Post-synthesis functionalization of MCM-41 microparticles

VS (1.0 mL) was added to a previously sonicated slurry of MCM-41 (1 g) in 50 mL of toluene, and kept under magnetic stirring at 70 °C for 24 h. The mixture was then extensively

washed with toluene and acetone to rinse away any residual chemicals. Finally, the powder was dried at 50 °C under vacuum for 24 h.

OES (1.9 mL) was added to a previously sonicated slurry of 1 g of mesoporous silica powder in 45 mL of toluene. The mixture was refluxed for 24 h under magnetic stirring. The solid was, then, filtered and washed with acetone, placed in a Soxhlet and extracted with acetone for 4 h. Finally, the powder was dried at room temperature under vacuum for 24 h.

2.4. Catalytic tests

Polymerizations were carried out in a 250 cm^3 dried and nitrogen-flushed bottle for pressure reactions (Wilmad LabGlass LG-3921) magnetically stirred, using toluene as solvent. Polymerizations were performed at 25ºC and 1.1 bar of ethylene. Temperature, ethylene consumption and pressure were monitored at real time using data acquisition and control software, enabling to obtain kinetic profiles. The polymerizations were run up to a specific amount of ethylene consumed. Polymerization mixtures were quenched by the addition of acidified methanol. The polymer was collected and washed twice with methanol before drying.

Two synthetic approaches are checked in order to evaluate the effect that catalyst immobilization on the silane-modified MCM-41 has on the ultimate characteristics of the resulting materials: method A, which consists of performing polymerization with the catalyst in a homogeneous medium; and method B, based on supporting the catalyst on silane-modified MCM-41. The supported catalysts prepared here show a zirconium load of 18.7 mmol/g MCM-41. The details of both methodologies can be found in the Supporting Information.

2.5. Characterization of neat and functionalized MCM-41 particles

All the samples were analyzed for phase identification by powder XRD in a Panalytical X'Pert Pro equipment, using CuKα radiation filtered by Ni and an X'Celerator detector.

Fourier Transform infrared (FTIR) spectra were recorded on a Thermo Nicolet Nexus instrument (64 scans with a resolution of 4 cm^{-1}). Self-supported wafers (≈10 mg) of MCM-41 powder were placed in an infrared quartz cell and then evacuated under primary vacuum (10^{-2} Torr) at 150 ºC. The background spectrum, recorded under identical operating conditions, was automatically subtracted from each sample spectrum.

Thermogravimetry measurements for characterizing the different MCM-41 microparticles were performed on a TGA 92 SETARAM under air atmosphere at a heating rate of 10 ºC/min. The mesoporous silica samples were fully hydrated before the analysis.

Nitrogen adsorption isotherms were measured at −196 ºC in ASAP 2010 Micromeritics equipment. Prior to the experiments, the unmodified MCM-41 sample was degassed at 300 ºC for 3 h while the modified samples of MCM-41 were degassed at 150 ºC for 7 h in order to prevent any organic degradation.

^{29}Si MAS NMR spectra were recorded on a Bruker Avance 400 spectrometer at 79.49 MHz, using 2.5 μs (equivalent to 40°) radiofrequency pulses, a recycle delay of 12 s and a spinning rate of 5.5 kHz.

2.6. Preparation of nanocomposite films

The nanocomposites based on silane-modified MCM-41 and HDPE were processed as films (thickness ca. 250-300 μm) by compression molding in a Collin press between hot plates at 170 ºC using a pressure of 2 MPa, for 4 min, and then cooled down to room temperature with circulating water. These films have been named as followed: HDPE/MCM41-VS-xh and HDPE/MCM41-VS-xs for those that use chloro(dimethyl)vinylsilane for functionalizing the MCM-41 particles and HDPE/MCM41-OES-xh and HDPE/MCM41-OES-xs for those that incorporate trimethoxy(7-octen-1-yl)silane. X is defined as MCM-41 wt. % content estimated by TGA and h an s are referred to polymerization performed under homogenous conditions or with supported catalyst, respectively.

2.7. Characterization of the nanocomposites

Scanning electron micrographs (SEM) were obtained on a JEOL JSM-7001F equipment. Transmission electron micrographs (TEM) images were obtained in a Hitachi H8100 equipment. Parallel cuts were prepared at -100 ºC for the TEM analysis of PE nanocomposites films from different samples using a LEICA EM FC6 cryo-camera in order to attain thin sections (80 nm) of the film surface by means of the LEICA EM UC6 ultramicrotome. Those cuts were picked up on cooper grids.

Wide-angle X-ray diffraction, WAXS, patterns used for characterizing the nanocomposites were recorded in the reflection mode by using a Bruker D8 Advance diffractometer provided with a PSD Vantec detector (from Bruker, Madison, Wisconsin). Cu Kα radiation (λ = 0.1542 nm) was used, operating at 40 kV and 40 mA. The parallel beam optics was adjusted by a parabolic Göbel mirror with horizontal grazing incidence Soller slit of 0.12° and LiF monochromator. The equipment was calibrated with different standards. A step scanning mode was employed for the detector. The diffraction scans were collected within the range of 2θ = 1–43°, with a 2θ step of 0.024° and 0.2 s per step.

Estimation of crystallinity (f_c) was carried out at room temperature from WAXS profile deconvolution into the crystalline diffractions and the amorphous component using a fitting program. The error in the crystallinity determinations is estimated to be ± 4 units.

Calorimetric analyses were carried out in a TA Instruments Q100 calorimeter connected to a cooling system and calibrated with different standards. The sample weights ranged from 5 to 7.5 mg. A temperature interval from -40 ºC to 160 ºC has been studied and the used heating rate was 10 ºC/min. For crystallinity determinations, a value of 290 J/g has been taken as the enthalpy of fusion of a perfectly crystalline material [20,21].

The degradation processes of the resulting nanocomposites were estimated by thermogravimetry using a TA Instruments TGA Q500 equipment working under inert and oxidant atmospheres. The equipment was calibrated according to standard protocols. The sample weights ranged from 4 to 6 mg, and the heating rate was 10 ºC/min.

Viscoelastic properties were measured in a Polymer Laboratories MK II dynamic mechanical thermal analyzer working in a tensile mode. The complex modulus and the loss tangent for each sample were determined at 1, 3, 10 and 30 Hz over a temperature range from -150 to 130 ºC, at a heating rate of 1.5 ºC/min.

Depth Sensing Indentation, DSI, experiments were performed at room temperature with a Shimadzu tester (model DUH211S) equipped with a Berkovich type diamond indenter. The experimental protocol consisted in the application of a load of 10 mN at a loading speed of 1.46 mN/s; the maintenance of this constant load for 5 s and, afterward, load was released with the

unloading speed equal than the one used along the loading stage. Finally, indentation depth was registered additionally for 5 s after reaching the minimum load (0.1 mN). Martens hardness, HMs, and indentation hardness, H_{it}, were calculated according to Oliver-Pharr method [22]. These hardness values are related to the ratio of the maximum load to the contact area under load and after releasing the indentor, respectively. Consequently, HMs is related to elastic, viscoelastic and permanent strains whereas H_{it} only depends on viscoelastic and plastic strains.

3. Results and discussion

3.1. Characterization of neat and functionalized MCM-41 particles

The grafting of the two organosilane coupling agents on the mesoporous silicas was monitored by ^{29}Si MAS NMR. The spectrum of neat MCM-41, depicted in Figure 1, displays two main resonance bands at -110 and -101 ppm, assigned to silicon sites Q^4 ($^*Si(OSi)_4$) and Q^3 ($HO^*Si(OSi)_3$) and a small shoulder at -92 ppm corresponding to a Q^2 environment (($HO)_2^*Si(OSi)_2$) [23]. The Q^3 and Q^2 sites correspond to isolated and geminal silanol groups respectively. The spectra of post-synthesis functionalized materials confirm the grafting of the silanes onto the MCM-41 surface through the appearance of new peaks that may be assigned to organosiloxane units: at 3 ppm associated with the silicon attached to VS groups [24]; and at -47 and -56 ppm corresponding to T^1 ($RSi(OSi)(OR')_2$, with $R'= CH_3$ or H) and T^2 ($RSi(OSi)_2(OR')$) sites for the OES modifier (Figure 1). For this latter case, the relative intensity of T1 and T2 peaks suggests that in average OES binds to 1.5 surface silanols.

The modification of MCM-41 particles with both silanes has been also observed by FTIR. Figure S1 of Supporting Information (SI) shows the FTIR spectra obtained for the neat mesoporous silica materials, MCM-41 (a); the post-synthesis decorated MCM-41 reacted with VS, MCM-41-VS (b); and the post-synthesis decorated MCM-41 reacted with OES, MCM-41-OES (c). The spectra were also normalized using the Si-O-Si overtones at about 1990 and 1875 cm^{-1} for a better comparison [25]. The spectrum of the neat MCM-41 support shows the typical features exhibited by mesoporous silicas with bands at about 3740 and 3500 cm^{-1} associated with OH stretching of isolated and interacting silanol groups [26], respectively, and bands at 2200-1600 cm^{-1}, corresponding to combination and overtone bands of Si-O network bonds. The

absence of physisorbed water can be easily assessed by the lack of H_2O bending mode frequency, normally observed at 1635 cm^{-1} (results not shown). After MCM-41 decoration with VS, the band at 3740 cm^{-1} ascribed to the surface isolated silanol groups almost disappears and new bands at 3057, 2966 and 1596 cm^{-1} are discernable. These bands might be ascribed to C-H stretching modes in double bonds and CH_3 groups and to C=C stretching mode, respectively. The spectrum of MCM-41 modified with OES also displays the complete disappearance of the band at 3740 cm^{-1} and the emergence of new bands at 3080, 2927, 2858 and 1641 cm^{-1}. These frequencies can be attributed to C-H stretching modes in double bonds and CH_2 groups and to C=C stretching mode, respectively. Furthermore, the disappearance of the Si-OH band confirms the covalent grafting of OES at the surface of the mesoporous support. Also, a shoulder at about 2970-2960 cm^{-1} can be seen, suggesting an incomplete hydrolysis of metoxy groups. This result is compatible with those attained by NMR measurements.

Figure S2 of SI depicts the N_2 adsorption isotherms obtained for either the neat or functionalized MCM-41 particles and Table 1 summarizes the textural parameters achieved from these experimental isotherms and the thermogravimetric data. MCM-41 particles exhibit a N_2 adsorption isotherm typical of mesoporous silicas (type IV), with the presence of a well defined pore filling step within a narrow range of p/p_0 (capillary condensation), demonstrating the fine organization of cylindrical pores of uniform size. Their post-synthesis modification with VS and OES silanes reduces the amount of N_2 adsorbed, as expected, but does not modify the isotherm type. Then, a decrease of the textural parameters of the support, S_{BET}, V_p, A_{ext} and D_p, is observed as result of MCM-41 functionalization. This reduction is more significant if OES is the interfacial agent used.

3.2. Polymerization activity

Incorporation of nanofillers into the polymerization media (*i.e.* direct contact with the cocatalyst (MAO) and the homogeneous metallocene catalyst in the reactor) might be a suitable approach for the obtainment of PE based nanocomposites by in situ polymerization. Polymerization activity is not expected to change significantly in absence of deactivating processes induced by the filler. Zapata et al. [27] have even recently referred to a slight increase

of ethylene polymerization activity when silica nanospheres are added together with the catalytic system directly in the polymerization reactor. Nevertheless, the addition under homogenous conditions of undecenoic acid as comonomeric unit to improve properties at polymer/MCM-41 interfaces has an opposite effect depending on its amount in the feed [17]: regular catalytic activity is achieved at contents low enough, while an important reduction is observed if undecenoic acid amount is raised in the feed. This behavior is due to the deactivating character of the carboxylic groups [28] and the incomplete protection that tri*iso*butylaluminum provides to those deactivating groups.

Table 2 reports high activity values for the ethylene polymerization performed with homogeneous Cp_2ZrCl_2 catalyst and using silane-decorated MCM-41 microparticles only as fillers. Thus, polymerization activity of ethylene is not significantly modified if MCM-41 particles are functionalized with silanes, these interfacial agents resulting, from this standpoint, more convenient than the use of other ones like undecenoic acid. Nevertheless, a significant decrease of the activity is observed upon Cp_2ZrCl_2 immobilization. This is a common feature in supported catalytic systems, especially for those obtained from direct impregnation methods. It is generally accepted in these cases that metallocenes are grafted on silica surface by elimination of chloride ligand with hydrogen atoms from silanol groups on the support, generating both monodentate and bidentate surface species. After MAO addition, monodentate μ-oxo surface species may be converted to active cationic sites for the polymerization of α-olefins [29-31]. Similar immobilization/activation processes are accepted for mesoporous silicas [10,32]. On the other hand, bidentate surface species (resulting from elimination of chloride ligand with hydrogen atoms of vicinal silanol groups) and binuclear species (resulting from bimolecular reaction between neighboring active centers) are inactive. The ratio between active and inactive species is dependent on surface density and distribution of OH groups. Figure S3 of SI represents the kinetic profiles obtained from the polymerization runs performed under heterogeneous conditions.

As it may be deduced from these plots, the average polymerization activity of the catalytic systems supported on MCM-41 modified with silanes is higher than the value obtained

10

for the supported catalyst on neat MCM-41 (580 kg PE/molZr.h). This behavior is in agreement with the reduction of the number of vicinal silanol groups that may deactivate the catalyst by the formation of bidentate species [33]. It is also clearly seen that activity reaches a maximum value, which is maintained along time on pristine MCM-41 and functionalized MCM-41-OES. A decay of catalytic activity behind the maximum is noticed if catalyst is supported on MCM-41-VS. This observation suggests a lower stability of the active species formed when MCM-41-VS particles are used

3.3. Structural and Morphological Characterization of Resulting Hybrids

Figure 2 shows the diffraction profiles at middle angle, MAXS, and wide angle, WAXS, at room temperature for different nanocomposites. It should be indicated that all of them have not been represented at middle angle (left plot) whereas the WAXS profiles have been shifted for clarity (right plot). It is undoubtedly noticeable from the left picture that the MCM-41 microparticles exhibits their characteristic mesoporous hexagonally arranged structure that consists of a strong reflection at around 2.2º and two weak reflections at 3.8º and 4.4º, which correspond to *(100)*, *(110)* and *(210)* diffraction planes of MCM-41, respectively (obviously, HDPE homopolymer does not display any signal in the MAXS region). The different silane functionalized nanocomposites present these diffractions of MCM-41, indicating that the well-ordered long-range structure is retained either if polymerization takes place under homogeneous (method A) or heterogeneous (approach B) conditions. Differences in intensity of the main *(100)* diffraction are dependent on the final MCM-41 content in the nanocomposite.

More details on the morphological characteristics exhibited by these materials can be obtained from TEM (see Figure 3) and SEM micrographs (Figure S4 of supporting information). These images provide additional knowledge about either particle distribution or size of agglomerates of the MCM-41 microparticles within the polyethylenic matrix. At an approximately similar VS silane content, it seems clear through TEM images that polymerization from support/filler surface seems to hamper agglomeration and promote particle filler dispersion. Thus, aggregates and particle distribution are of smaller size and more homogeneous, respectively, as deduced if the HDPE/MCM41-VS-8h and HDPE/MCM41-VS-

9s specimens are compared. Good morphological features seem also to be observed in the supported HDPE/MCM41-OES-7s sample. Nevertheless, conclusions are somehow different if images are taken with lower magnification, i.e., through SEM pictures. The HDPE/MCM41-VS-9s material seems again to be better than HDPE/MCM41-VS-8h. However, two clear zones are distinguished in the HDPE/MCM41-OES-7s material: some regions with a high content of inorganic components and other ones where MCM-41 is rather absent. Accordingly, heterogeneity in this HDPE/MCM41-OES-7s seems to be globally superior to that exhibited by the other two samples. The formation of these agglomerates might be favored because of the development of crosslinkings. These can take place through the OES double bonds under the applied experimental conditions (heated under reflux for 24 h with stirring).

Moreover, a fibrous-like structure, randomly disseminated, is markedly seen in Figure 3 for all of the materials as well as the existence of some aggregates of MCM-41 with different sizes. These tubular-like arrangements [34] are generated by the MCM-41 hexagonal long channels, these tubules being coated by polyethylene macrochains. Then, polyethylene based macromolecules would be located either within the MCM-41 long channels or wrapping them outside.

Coming back to Figure 2, its right plot represents the X ray profiles at wide angle region, WAXS, for the distinct silane decorated hybrids. At room temperature, all of them show the orthorhombic lattice common in polyethylene and derivatives, characterized by the two main *(110)* and *(200)* diffractions [35,36]. It is clear from the WAXS profiles that location of these two primary diffractions is rather unvarying for the different samples and, consequently, dimensions of crystal lattice remain practically unaffected in these diffraction planes by incorporation of silane-functionalized MCM-41 microparticles. A decrease in diffraction intensity is, however, observed when hybrids are compared with HDPE, this effect being more evident for composites with the highest MCM-41 contents (*i.e.*, HDPE/MCM41-VS-23h, HDPE/MCM41-VS-28s and HDPE/MCM41-OES-25s). This reduction should be associated, at first glance, with a diminishment in crystallinity as function of MCM-41 content.

12

The degree of crystallinity can be quantified from deconvolution of the different WAXS profiles into the crystalline diffractions and amorphous halo (as commented in the Experimental Section). However, the WAXS profile of pure MCM-41 shows a broad diffraction centered at around $2\theta = 23°$ (see upper insert in right plot of Figure 2), so that the simple deconvolution into crystalline diffractions and amorphous counterpart is leading to underestimation of the real polyethylene crystallinity. Accordingly, the subtraction of the actual MCM-41 amount present at a specific material has to be performed previous the deconvolution in the HDPE pattern. Once the MCM-41 contribution has been kept out, the crystallinity values are determined, being reported in Table 3. A noticeable decrease of the WAXS crystallinity is observed when MCM-41 is present, especially evident for those hybrids with the highest MCM-41 contents.

Figure 4 shows the normalized DSC curves during the first melting run for all of the specimens, *i.e.*, those calorimetric traces account the actual amount of HDPE in the composites. Several characteristics can be deduced, as follows. The first one is correlated to the noticeable presence of a secondary endothermic process in the different hybrids (no signal of it is seen in HDPE) at around 75-80 ℃ as well as the main melting peak located at about 133 ℃. This minor melting process is considerable more important as MCM-41 content increases in the nanocomposite, as visibly deduced from the inset. It is obvious that the process at lower temperatures involves the melting of crystallites with significantly smaller size. These thinner crystals are probably the ones developed from the polymeric chains that are included into the MCM-41 channels and are not able to grow further within those channels because of confinement effects. Consequently, its intensity increases as MCM-41 does since the amount of polymeric matrix becomes greater within these channels.

The melting enthalpies (and DSC crystallinities) of these hybrids show two interesting features. Firstly, the total crystallinity determined from these initial DSC runs is the same for the different hybrids, as listed in Table 3 and depicted in Figure 5 (except for the specimen HDPE/MCM41-OES-7s that shows an anomalous low degree of crystallinity). This stands in contrast to the significant decrease observed in the WAXS crystallinity. Second, if the enthalpy involved in the secondary process is excluded, then a rather similar variation is obtained

between the crystallinity deduced from the main melting peak at around 133 °C and that observed from X-ray crystallinity (f_c^{WAXS}) estimation, as clearly seen in Figure 5. Accordingly, it can be assumed that these very small entities that melt at around 70-85 ºC lead to rather wide diffraction peaks that are not well accounted for in the X-ray crystallinity, f_c^{WAXS}. This fact together with the constancy of total crystallinity determined from first DSC runs was preliminary identified in the nanocomposites that incorporated undecenoic acid as interfacial agent [17]. Once the enthalpy corresponding to that minor melting process is subtracted, trends observed for both techniques are rather analogous (see Figure 5), these results now confirming those previous assumptions.

It seems to be deduced, therefore, that the enthalpy arising from the PE chains confined inside the MCM41 channels (see $f_c^{DSC}{}_{CONFINEMENT\ PEAK}$ in Figure 5 and Table 3) increases more or less linearly with the total MCM-41 content, up to around a 10% of total crystallinity for sample HDPE/MCM41-VS-28s, although a certain dependence on the type of silane seems to be observed (see below).

The assumption of rather wide diffraction peaks can be ascertained from a straightforward determination of the expected width of those peaks by employing the Scherrer equation [37]. Thus, the width at half maximum of the diffractions for a crystal length of 2 nm (on the order of the pore diameters) should be around 4 degrees in 2θ. Such high values will in fact prevent the observation of real diffraction peaks.

Regarding the melting temperatures of such very thin crystals, some estimation can be also made by means of the Gibbs-Thomson equation. Most usually, a simplified version of that equation is employed [38-40] when dealing with lamellar crystals of finite size along the macromolecular chain but with very large sizes for the lateral dimension. In the present case, however, a more general equation is needed [41,42] since the macromolecules confined in the channels of MCM-41 are supposed to have rather reduced lateral dimensions, similar to the diameter of the pores.

Such equation relates the observed melting temperature, T_m, with the dimensions of the crystal as follows:

14

$$T_m = T_m^0 \left[1 - \left(\frac{\gamma_1}{L_1} + \frac{\gamma_2}{L_2} + \frac{\gamma_3}{L_3} \right) \frac{2}{\Delta h_f^0} \right]$$

where T_m^0 is the equilibrium melting temperature of the crystal with infinite thickness, L_1, L_2 and L_3 are the three dimensions of the crystallite and γ_1, γ_2 and γ_3, the corresponding surface free energies in those directions, while Δh_f^0 is the heat of fusion per unit volume. Somewhat different values are given in the literature for either the surface free energies or for T_m^0. Nevertheless, by using the following values: $T_m^0 = 418.7$ K, $\gamma_1 = 90$ erg/cm^2, $\gamma_2 = \gamma_3 = 14$ erg/cm^2, and $\Delta h_f^0 = 280$ J/cm^3 and assuming that $L_1 = 10$ nm, then the extreme values of the endotherm assigned to the confined crystals, which are 82 and 74 °C (see inset in Figure 4), are corresponding to values of $L_2 = L_3 = 2.3$ and 1.9 nm, respectively. The results amount to 1.7 and 1.5 nm if L_1 is assumed to be 20 nm. In any case, these values are very similar to the average pore diameters for MCM-41-VS and MCM-41-OES reported in Table 1.

It is also interesting to remark the significant reduction in crystallinity of this "secondary" process after cooling from the molten state and subsequent heating scans (second melting) in all the specimens. This fact is clearly observed in Figure S5 for the HDPE/MCM41-VS-28s and HDPE/MCM41-OES-25s samples, with the highest MCM-41 contents. This feature suggests that there is a delay in the development of those ordered entities within MCM-41 channels in the nanocomposites, which cannot be generated in the same extent and size during the experimental time because of confinement effects, as deduced from the smaller area and the shift of that secondary peak to lower temperatures. Nevertheless, crystallites outside the channels present a size higher than the one exhibited by those crystals melting during the first heating run, as demonstrated by the slight increase of their melting temperatures (see T_m^{F2} values in Table 3). This shift is associated with the smaller rate of crystallization applied during DSC experiments (10 °C/min) compared with that fast cooling imposed along the initial processing (80-100 °C/min), the former one allowing a large crystal perfection.

Another characteristic that can be derived from Figure 4 (see the inset) is the apparent dependence of the intensity of this confinement peak on the type of silane used for the

decoration of the MCM-41. It seems evident when comparing HDPE/MCM41-VS-23h or HDPE/MCM41-VS-28s and HDPE/MCM41-OES-25s specimens that more polyethylene chains are able to go within the channels and, then, to crystallize if MCM-41 microparticles are post-modified with VS instead of OES. This fact can be ascribed to the different parameters of these mesoporous MCM-41 particles functionalized with those two silanes. The higher steric hindrance associated with OES leads to particles with lower specific surface area and specific pore volume as well as smaller external area and a smaller average pore diameter (see table 1), turning out more difficult for polyethylene chains to polymerize within the channels. Nevertheless, intensity of this confinement peak seems to be rather independent of the in situ polymerization taking place under homogeneous or heterogeneous conditions.

This thermal behavior here observed is somehow different to that previously found in the literature for similar nanocomposites [43]. The reason for such variations may be due to the fact that those nanocomposites were analyzed from the as-prepared reactor powders, *i.e.*, the sample obtained just after polymerization, which basically consists in extended-chain nanofibrils [21,44] whereas the hybrids here analyzed have been further processed as films, and the majority conformation is not in the form of extended-chain but as random coil.

3.4. Thermal Stability of Resulting Hybrids

The knowledge of the decomposition behavior of these nanocomposites is required for their further applicability since MCM-41 is, sometimes, used as catalyst of degradation processes [45] and these materials were exposed to temperature during film preparation by melt processing. It is, then, mandatory to evaluate if that processing from the molten state affects or not the resulting thermal stability or if decomposition has been initiated. Melt processing has been chosen to prepare films because it is a cost-effective and an environmentally-friendly method, which avoids the use of any solvent. Furthermore, the amount of inorganic solids can also be estimated from the thermogravimetric curves. The results show that content determined at a given specimen is rather independent of the environment used. The average values obtained from inert and oxidative conditions are listed in Tables 2 and 3.

16

Figure 6 shows the thermogravimetry curves under air and inert environments for the different hybrids. Under inert conditions (right plots), a single primary stage of decomposition is observed in the temperature range from 200 to 650 ℃ for all specimens. Thermal decomposition of neat polyethylene has been reported to occur under these conditions through a random scission mechanism that turns out in the fragmentation of original polymeric chain into fragments of varying length. The mechanism describes a random generation of free radicals along the polymer backbone, followed by the scission of the molecule that results in the formation of a molecule with an unsaturated end and another with a terminal free radical. Subsequent hydrogen chain transfer reactions transform the radical fragments into straight chain dienes, alkenes and alkanes [46].

On the contrary, several different degradation processes are noticeable in the different hybrids and the homopolymer, at identical temperature interval, when air is the environment used (represented in the left plots of Figure 6). It is well known that the initial reaction of the polyethylene thermal oxidation is the formation of alkyl radicals from polymeric chains. And the next stage is the reaction of alkyl radicals with oxygen to form hydroperoxides, which can decompose to alkoxyl radicals. Then, the alkoxyl radicals abstract hydrogen from the chain and other alkyl radical forms. Finally, various carbonyl species are generated.

The presence of MCM-41 microparticles decorated with silanes in the nanocomposites has markedly an effect of degradation promoter under both atmospheres used. Thus, the beginning of decomposition takes place in the different hybrids at temperatures lower than in the HDPE homopolymer, as listed in Table 4 and represented in Figure S6 of Supporting Information for the $T_{5\%}$ and $T_{20\%}$ mass losses. As degradation is further progressing ($T_{50\%}$), species more stable than those in the HDPE are, however, generated in some of the nanocomposites with MCM-41 contents lower than 10 wt.%.

In addition, and for a given silane, those nanocomposites prepared with the supported catalyst degrade in an inert environment more easily than those obtained using the catalyst in a homogeneous medium, because some traces of catalyst might be probably trapped within MCM-41 channels, favoring degradation. Furthermore, OES provides higher stability than VS

17

under inert conditions. These two last features are not observed under air condition probably because of the great complexity of processes involved in oxygen presence.

3.5. Mechanical Behavior of Resulting Hybrids

Figure 7 shows the variation of the storage and loss moduli as well as of the loss tangent for the HDPE and the different nanocomposites, from DMTA measurements. In the two upper plots, an increase of the storage modulus is observed when MCM-41 microparticles are incorporated if compared with the modulus exhibited by the neat HDPE. The highest values are presented by the two nanocomposites with the largest MCM-41 contents, *i.e.*, HDPE/MCM41-VS-28s and HDPE/MCM41-OES-25s. This increase in stiffness observed in the nanocomposites should be mainly ascribed to the inherent reinforcement effect of the mesoporous filler since DSC crystallinity values (estimated from films during their first heating run) are rather similar in the different hybrids with exception of the HDPE/MCM41-OES-7s. Furthermore, it is noticeable that this improvement in rigidity with MCM-41 content is more important above room temperature, that is, when the mobility within the olefinic polymer chains increases, as can be clearly seen in Figure 7. A similar mechanical response has been also found from Depth Sensing Indentation measurements and the corresponding indentation hardness, H_{it}, values obtained (see Table 5). Hardness of a material can be defined as a measurement of the resistance to a permanent deformation or damage. The equipment used for this study is able to perform and monitor loading-maintenance-unloading processes, as seen in Figure 8 for all of the hybrids. The two nanocomposites with the largest MCM-41 microparticle contents, i.e., HDPE/MCM41-VS-28s and HDPE/MCM41-OES-25s, are the hardest materials, and, consequently, the indenter cannot penetrate too much in its surface. The HDPE/MCM41-VS-23h is slightly softer than those just mentioned, and thus indenter penetration is slightly enlarged. As MCM-41 composition is reduced, materials become significantly more deformable and indenter goes deeper inside. There is not too much difference between these low MCM-41 content samples, with the exception of the HDPE/MCM41-OES-7s that is the softest one, due probably to its lower crystallinity. Accordingly, the two parameters that mainly trigger hardness, in particular, and the mechanical response, in general, are MCM-41 content and HDPE

18

crystallinity. The influence of crystallinity in hardness values has been also found in other olefinic based polymers [47-50]. Effect of other morphological features, as particle agglomeration and dispersion heterogeneity among others, does not show straightforward trends on mechanical response and the obtained information may be sometimes contradictory. As well, an easy correlation of rigidity on the preparation approach and on the silane type used for MCM-41 modification cannot be unambiguously established, probably because analogous polymer-filler interactions are developed within the hybrids (in agreement with data shown in an earlier article [16]) and, then, similar effects turn out in the compatibilization of the two different phases. It can be only said that at the highest MCM-41 contents, nanocomposites prepared using the catalyst supported on the mesoporous microparticles seem to exhibit larger stiffness. For those highest contents a three-fold increase both on storage modulus and hardness may be attained under specific conditions (samples HDPE/MCM41-VS-28s).

In relation to relaxation processes, the *tan δ* and *E''* representations in Figure 7 display the existence of two main processes, labeled as *γ* and *α* in order of increasing temperatures. Intensity and location are slightly dependent on MCM-41 content, as noticed from *tan δ* plot. The other common relaxation, named as *β* and located between the *γ* and the *α* processes in low density polyethylene, linear low density polyethylene and ethylene copolymers [7,9,51,52] is not clearly observed for these specimens. The crystallinity of these samples is relatively high and, therefore, that relaxation process is almost absent and overlapped with the *α* mechanism, corroborating similar features found in other HDPE samples [53].

The *γ* relaxation in polyethylene was firstly attributed to crankshaft movements of polymethylenic chains [54]. However, there is no clear consensus regarding the details of the underlying motional process [55]. This type of motion requires chains within the amorphous phase containing sequences of three or more methylenic units. Figure 7 and data in Table 5 show that the location of *γ* loss modulus peak is not significantly affected by the MCM-41 content, but its intensity decreases since there is less polyethylene that contributes to this relaxation as MCM-41 microparticles amount increases.

The relaxation that appears at higher temperature, α relaxation, has been associated with vibrational and reorientational motions within the crystallites [56,57]. At the highest temperatures, the melting of the crystallites is overlapped with this relaxation process. As discussed for the motions within the amorphous regions, the mobility occurring in the crystals also becomes more restricted as the MCM-41 content increases and, consequently, the location of the α relaxation is shifted to higher temperatures and its broadness is enlarged involving wide relaxation time distributions, as clearly seen from E'' representations (lower plots in Figure 7). Furthermore, its intensity is reduced, more clearly noticeable from the $tan \, \delta$ plot (in fact, this is the independent experimental parameter since E'' is estimated from storage modulus, E', and $tan \, \delta$ values).

Additional information on the mechanical performance of these hybrid materials can be attained from these loss magnitudes since they are related to viscoelastic energy dissipation, which is expected to make a significant contribution in the impact energy because the time scale involved in impact deformation is of comparable order of magnitude as the relaxation time of viscoelastic processes. Therefore, correlation of impact strength with dynamic mechanical behavior has been previously reported [58-62]. The area under the loss tangent curve provides an estimation of the impact strength, although it is not a direct measurement. In the present investigation, the region integrated has been that from -50 to 125 ℃ and the values obtained are listed in Table 5. As expected, a decrease of area is observed, indicating that the nanocomposites are able to absorb less energy before breaking as MCM-41 content increases. However, it is noticeable that this reduction is much smaller than the increase in elastic modulus, fact that seems to point out that a favorable compromise between these two opposite mechanical characteristics is reached.

4. Conclusions

New materials based on commodity polyethylene and MCM-41 microparticles, synthesized by several approaches using silanes as interfacial agents, have been prepared in order to improve their ultimate mechanical properties through increasing interfacial contact between the two components. Concerning the catalytic aspects, the modification of MCM-41

with silane was found to lead to a beneficial effect in terms of the polymerization activity of the supported catalyst when compared to the analogous supported system on pristine MCM-41. Moreover, changes on active species stability seem to occur when changing from MCM-41-OES to MCM-41-VS supports. The latter one seems to give rise to less stable species.

Regarding dispersion of filler particles within polyethylene-based matrix, it appears that aggregates are of smaller size and distributed more homogeneously in the hybrids where MCM-41 acts as catalyst carrier as well as filler.

Independently of the preparation methodology used, the PE nanocomposites based on MCM-41 microparticles decorated with silanes maintain the well-ordered initial long-range features of those mesoporous materials. This fact indicates that the polyethylene macrochains within the pores and channels do not significantly alter the original MCM-41 structure observed at the MAXS region.

The existence of a secondary endothermic process in the nanocomposites at around 80 ºC points out the presence of crystallites with significantly smaller size in addition to those thicker ones that melt at around 130 ºC. The small endothermic transition found in the nanocomposites has been ascribed to the melting of the polymeric chains located within channels that make up the MCM-41 microparticles. A delay in the development of those ordered entities is observed for the highest contents, probably due to confinement effects.

Decomposition process begins at lower temperatures in the hybrids compared with that exhibited by neat HDPE. That shift is more noticeable at the highest MCM-41 contents, independently of the atmosphere used for the measurements.

The type of the silane used for MCM-41 modification does not affect significantly rigidity of the different materials suggesting that the ability of the tested silanes to promote the adhesion and compatibility between the two different phases is similar. A rigidity enhancement is clearly seen from the increase of both the storage modulus and hardness values. A three-fold increase on these magnitudes was observed for the two nanocomposites prepared under supported conditions and containing the highest contents of MCM-41. Moreover, a mobility

21

reduction is deduced from the decrease of relaxation intensities in those hybrids with around 25 *wt*.% MCM-41 content and specially for those obtained from the supported catalyst.

Then, ultimate mechanical performance improves with MCM-41 incorporation without varying the final processing temperature.

References

1. A.M. Diez-Pascual, M. Naffakh, C. Marco, G. Ellis, M.A. Gomez-Fatou, Prog. Mater. Sci. 57 (2012) 1106.
2. H.W. Ha, A. Choudhury, T. Kamal, D. H.Kim, S.Y. Park, ACS Appl. Mater. Inter. 4 (2012) 4623.
3. (a) J. Arranz-Andrés, M.L. Cerrada, Sci.Adv. Mater. 5 (2013) 1; (b) J. Arranz-Andrés, E. Pérez, M.L. Cerrada, Sci.Adv. Mater. 5 (2013) 1524.
4. M.L. Cerrada, C. Serrano, M. Sánchez-Chaves, M. Fernández-García, F. Fernández-Martín, A. de Andrés, R.J. Jiménez Riobóo, A. Kubacka, M. Ferrer, M. Fernández-García, Adv. Funct. Mater. 18 (2008) 1949
5. A. Kubacka, M.L. Cerrada, C. Serrano, M. Fernández-García, M. Ferrer, M. Fernández-Garcia, J. Phys. Chem. C 113 (2009) 9182.
6. A. Kubacka, M. Ferrer, M. Fernández-García, C. Serrano, M.L. Cerrada, M. Fernández-García, Appl. Catal. B-Environ. 104 (2011) 346.
7. J. Fox, J.J. Wie, B.W.Greenland, S. Burattini, W. Hayes, H.M. Colquhoun, M.E. Mackay, S.J. Rowan, J. Am. Chem. Soc. 134 (2012) 5362.
8. M.L. Cerrada, R. Benavente, E. Pérez, J. Moniz-Santos, M.R. Ribeiro, Polymer 42 (2001) 7197.
9. M.L. Cerrada, R. Benavente, E. Pérez, Macromol. Chem. Phys. 203 (2002) 718.
10. J.M. Campos, J.P. Lourenço, H. Cramail, M.R. Ribeiro, Prog. Polym. Sci. 37 (2012) 1764.
11. K. Kageyama, J. Tamazawa, T. Aida, Science 285 (1999), 2113.
12. Z.B. Ye, S.P. Zhu, W.J. Wang, H. Alsyouri, Y.S. Lin, J. Polym. Sci. Polym. Phys. 41 (2003) 2433.
13. J.S. Beck, J.C. Vartuli, W.J. Roth, M.E. Leonowicz, C.T. Kresge, K.D. Schmitt, C.T.W. Chu, D.H. Olson, E.W. Sheppard, S.B. McCullen, J.B. Higgins, J.L. Schlenker, J. Am. Chem. Soc. 114 (1992) 10834.
14. M.L. Cerrada, E. Perez, J.P. Lourenco, J.M. Campos, M.R. Ribeiro, Micropor. Mesopor. Mat. 130 (2010) 215.
15. J.M. Campos, J.P. Lourenço, E. Perez, M.L. Cerrada, M.R. Ribeiro, J. Nanosci. Nanotechno. 9 (2009) 3966.
16. A. Bento, J.P. Lourenço, A. Fernandes, M.R. Ribeiro, J. Arranz-Andrés, V. Lorenzo, M.L. Cerrada, J. Membr. Sci. 415–416 (2012) 702.

17. María L. Cerrada, Ernesto Pérez, João P. Lourenço, Artur Bento, M. Rosário Ribeiro, Polymer 54 (2013) 2611

18. O.H. Lin, H.M. Akil, Z. A.M. Ishak, Polym. Comp. 32 (2011) 1568.

19. J.P. Lourenco, A. Fernandes, C. Henriques, M.F. Ribeiro, Micropor. Mesopor. Mat. 94 (2006) 56.

20. F.A. Quinn, L. Mandelkern, J.Am. Chem. Soc. 80 (1958) 3178.

21. B. Wunderlich, Macromol. Physics. New York: Academic Press, 1980.

22. W.C. Oliver, G.M. Pharr, J. Mater. Res. 7 (1992) 1564.

23. D.W. Sindorf, G.E. Maciel, J. Am. Chem. Soc. 103 (1981) 4263.

24. X.S. Zhao, G.Q. Lu, A.K. Whittaker, G.J. Millar, H.Y. Zhu, J. Phys. Chem. B 101 (1997) 6525.

25. A. Jentys, K. Kleestorfer, H. Vinek, Micropor. Mesopor. Mat. 27 (1999) 321.

26. J. Chen, Q. Li, R. Xu, F. Xiao, Angew. Chem. Int. Edit. 34 (1996) 2694.

27. P. A. Zapata, R. Quijada, I. Lieberwirth, R. Benavente, Macromol. React. Eng. 5 (2011) 294.

28. M.L. Cerrada, R. Benavente, E. Pérez, J. Moniz-Santos, J.M. Campos, M.R. Ribeiro, Macromol. Chem. Phys. 208 (2007) 841.

29. W.C. Finch, R.D. Gillespie, D. Hedden, T.J. Marks, J. Am. Chem. Soc. 112 (1990) 6221.

30. M. Jezequel, V. Dufaud, M.J. Ruiz-Garcia, F. Carrillo-Hermosilla, U. Neugebauer, G.P. Niccolai, F. Lefebvre, F. Bayard, J. Corker, S. Fiddy, J. Evans, J.P. Broyer, J. Malinge, J.M. Basset, J. Am. Chem. Soc. 123 (2001) 3520.

31. N. Millot, S. Soignier, C.C. Santini, A. Baudouin, J. M. Basse, J. Am. Chem. Soc. 128 (2006,) 9361.

32. C. Alonso-Moreno, D. Perez-Quintanilla, D. Polo-Ceron, S. Prashar, I. Sierra, I. del Hierro, M. Fajardo, J. Mol. Catal. A−Chem. 304 (2009) 107.

33. J.H.Z. dos Santos, P.P. Greco, F.C. Stedile, J. Dupont, J. Mol. Catal. A−Chem. 154 (2000) 103.

34. A. Chenite, Y. Le Pag, A. Sayari, Chem. Mater. 7 (1995) 1015.

35. K. Shirayam, H. Watabe, S. Kita, Makromol. Chem. 151 (1972) 97.

36. C.W. Bunn, Transactions of the Faraday Society 40 (1944) 23.

37. L.E. Alexander, X-Ray Diffraction Methods in Polymer Science, Wiley, New York, 1969, p. 335.

38. B. Wunderlich, 'Macromolecular Physics', Vol. 3, 'Crystal Melting', Academic Press, New York, 1980, p. 30.

39. O. Darras, R. Séguéla, Polymer 34 (1993) 2946.

40. L. Lu, R.G. Alamo, L. Mandelkern, Macromolecules 27 (1994) 6571.

41. U.W. Gedde, Polymer Physics; Chapman & Hall: London, 1995.

42. K. Shin, E. Woo, Y.G. Jeong, C. Kim, J. Huh, and K-W. Kim, Macromolecules 40 (2007) 6617.

43. K. Kageyama, J. Tamazawa, T. Aida, Science 285 (1999) 2113.

44. S. Chen, C. Guo, L. Liu, H. Xu, J. Dong, Y. Hu, Polymer 46 (2005)1093.

45. A. Marcilla, A. Gomez-Siurana, D. Berenguer, Appl, Catal, A−Gen. 301 (2006) 222.

46. F.S.M. Sinfrônio, A.G. Souza, Ieda M. G. Santos, V.J. Fernandes Jr., Cs. Novák, Zsuzsanna Éhen, J. Therm. Anal. Calorim., 85 (2006) 391.

47. J. Arranz-Andrés, J.L. Guevara, T. Velilla, R. Quijada, R. Benavente, E. Pérez, M.L. Cerrada, Polymer 46 (2005) 12287.

48. J.M. López-Majada, H. Palza, J.L. Guevara, R. Quijada, M.C. Martínez, R. Benavente, J.M. Pereña, E. Pérez, M.L. Cerrada, J. Polym. Sci. Polym. Phys. 44 (2006)1253.

49. a) H. Palza, J.M. López-Majada, R. Quijada, R. Benavente, Pérez E, M.L. Cerrada, Macromol. Chem. Phys. 206 (2005) 1221; b) H. Palza, J.M. López-Majada, R. Quijada, J.M. Pereña, R. Benavente, E. Pérez, M.L. Cerrada, Macromol. Chem. Phys. 209 (2008) 2259.

50. C. Fonseca, J.M. Pereña, R. Benavente, M.L. Cerrada, A. Bello, E. Pérez, Polymer 36 (1995) 1887.

51. a) R. Popli, M. Glotin, L. Mandelkern, R.S. Benson, J. Polym. Sci. Polym. Phys. 22 (1984) 407; b) R. Popli, L. Mandelkern. Polym. Bull. 9 (1983) 260.

52. M.L. Cerrada, J M. Pereña, R. Benavente, E. Pérez, Polymer 41 (2000) 6655..

53. M.L. Cerrada, R. Benavente, B. Peña, E. Pérez, Polymer 41 (2000) 5957.
54. T.F. Schatzki, J. Polym. Sci. 57 (1962) 337.
55. R.H. Boyd, Polymer 26 (1985) 1123.
56. I.M. Ward, Mechanical Properties of Solid Polymers, 2nd ed. Chichester: J. Wiley and Sons, 1983.
57. B. McCrum, B. Read, G. Williams. Anelastic and Dielectric Effects in Polymeric Solids. New York: Dover Publications, 1991.
58. P.I. Vincent, Polymer 1 (1960) 425.
59. J. Heijboer, J. Polym. Sci. Polym. Symp. 16 (1967) 3755.
60. A. Hiltner, E. Baer, Polymer 15 (1974) 805.
61. S.H. Jafari, A.K. Gupta, J. Appl. Polym. Sci. 78 (2000) 962.
62. O. Prieto, J.M. Pereña, R. Benavente, E. Pérez, M.L. Cerrada, J. Polym. Sci. Polym. Phys. 41 (2003) 1878.

Table 1. Parameters of the MCM-41 mesoporous materials used as fillers and/or supports.

Sample	Modifying agent content (mmol/g)	Silane weight loss % (w/w) [a]	S_{BET} (m^2/g)	V_p [b] (cm^3/g)	A_{Ext} [b] (m^2/g)	D_p [c] (Å)
MCM-41	-	-	873	0.68	44	28
MCM-41-VS	7.5	5,2	757	0.50	42	23
MCM-41-OES	7.5	13	576	0.32	20	17

S_{BET}: specific surface area; V_p: specific pore volume; A_{Ext}: external area; D_p: average pore diameter estimated.
[a] Determined from TGA.
[b] Calculated using the t-plot method. It corresponds to mesoporous volume for the samples.
[c] Calculated using the Barrett–Joyner–Halenda (BJH) method.

25

Table 2. Polymerization conditions and activities obtained for the synthesis of HDPE/MCM41 hybrids[a].

Sample	Support/Filler	Method	Zr loading (μmol/g)	[Zr] (10^{-5}M)	Activity (kg PE/ mol Zr . h)	Filler content[c] (wt. %)
HDPE	-	H	-	3.8	13700	-
HDPE/MCM41-VS-8h	MCM-41-VS	H	-	3.8	13020	8
HDPE/MCM41-VS-23h[b]	MCM-41-VS	H	-	3.8	10340	23
HDPE/MCM41-VS-9s	MCM-41-VS	S	6	1.2	650	9
HDPE/MCM41-VS-28s[b]	MCM-41-VS	S	6	2.4	1250	28
HDPE/MCM41-OES-7h	MCM-41-OES	H	-	3.8	13077	7
HDPE/MCM41-OES-7s	MCM-41-OES	S	12	2.4	830	7
HDPE/MCM41-OES-25s[b]	MCM-41-OES	S	12	4.8	430	25

[a] $P_{ethylene}$ = 1.2 bar, T = 25 ºC, Al/Zr=1000, weight of MCM-41 = 100 mg; [b]: weight of MCM-41 = 200 mg. [c] Obtained by TGA; H: Homogeneous catalyst, S: Supported catalyst

26

Table 3. Average MCM-41 *wt*.% content estimated by thermogravimetry (TGA); crystallinity estimated from WAXS, f_c^{WAXS}; normalized crystallinity, f_c^{DSC}, as well as transition temperatures, T_m and T_c, determined from differential scanning calorimetry, DSC, for first melting, crystallization and second melting, F1, C and F2, respectively. The $f_c^{DSC}{}_{F1}{}^{CONF}$ and $f_c^{DSC}{}_{F1}{}^{EXT}$ columns are related to crystallinity within and out the MCM-41 hexagonal arrangements, respectively.

Sample	MCM-41 content ($wt.\%^{TGA}$)	f_c^{WAXS}	$f_c^{DSC}{}_{F1}{}^{TOTAL}$	$f_c^{DSC}{}_{F1}{}^{CONF}$	$f_c^{DSC}{}_{F1}{}^{EXT}$	T_m^{F1} (ºC)	$f_c^{DSC}{}_{C}{}^{TOTAL}$	T_c (ºC)	$f_c^{DSC}{}_{F2}{}^{TOTAL}$	T_m^{F2} (ºC)
HDPE	0	0.64	0.59	0.00	0.59	133.5	0.59	119.5	0.59	134.0
HDPE/MCM41-VS-8h	8	0.55	0.58	0.05	0.53	133.5	0.58	120.5	0.58	134.5
HDPE/MCM41-VS-23h	23	0.50	0.58	0.09	0.49	133.5	0.56	119.5	0.56	134.5
HDPE/MCM41-VS-9s	9	0.55	0.58	0.04	0.54	133.5	0.55	119.5	0.55	134.0
HDPE/MCM41-VS-28s	28	0.42	0.58	0.10	0.48	133.0	0.50	121.0	0.50	134.5
HDPE/MCM41-OES-7h	7	0.56	0.58	0.01	0.57	132.0	0.59	120.0	0.59	135.0
HDPE/MCM41-OES-7s	7	0.52	0.46	0.02	0.44	134.0	0.46	120.0	0.46	133.5
HDPE/MCM41-OES-25s	25	0.47	0.58	0.07	0.49	132.5	0.51	121.0	0.51	134.0

Table 4. Thermogravimetric results: average MCM-41 *wt*.% content and characteristic decomposition temperatures at specific mass loss (5% $-T_{5\%}-$, 20% $-T_{20\%}-$ and 50% $-T_{50\%}-$) under both oxidant and inert atmospheres for all the specimens.

Sample	MCM-41 content ($wt.\%^{TGA}$)	Oxidant atmosphere			Inert atmosphere		
		$T_{5\%}$ (ºC)	$T_{20\%}$ (ºC)	$T_{50\%}$ (ºC)	$T_{5\%}$ (ºC)	$T_{20\%}$ (ºC)	$T_{50\%}$ (ºC)
HDPE	0	310.0	403.5	418.5	446.0	465.0	478.5
HDPE/MCM41-VS-8h	8	288.5	341.0	430.5	418.5	443.5	460.0
HDPE/MCM41-VS-23h	23	258.5	283.0	351.5	391.0	419.0	443.0
HDPE/MCM41-VS-9s	9	287.5	325.5	437.0	370.5	406.5	434.0
HDPE/MCM41-VS-28s	28	258.5	288.0	364.5	363.5	390.0	413.5
HDPE/MCM41-OES-7h	7	276.5	331.5	432.5	442.5	463.5	476.5
HDPE/MCM41-OES-7s	7	295.0	359.0	428.5	413.0	442.0	459.5
HDPE/MCM41-OES-25s	25	260.0	300.0	383.5	365.5	404.0	435.0

Table 5. Relaxation temperature for the two relaxation processes (in E'' basis), storage modulus value at 25 ºC and area under tan δ curves from -50 to 150 ºC in the different nanocomposites at 3 Hz. Hit is referred to values of indentation hardness at 25 ºC.

sample	MCM-41 ($wt.\%^{TGA}$)	T (ºC) γ	T (ºC) α	$E'_{25\,ºC}$ (MPa)	$tan\,\delta$ area (a. u.)	H_{it} (MPa)
HDPE	0	-112	50	710	22	47.5
HDPE/MCM41-VS-8h	8	-112	52	1220	19	74.2
HDPE/MCM41-VS-23h	23	-114	64	1670	16	94.0
HDPE/MCM41-VS-9s	9	-111	60	950	18	70.0
HDPE/MCM41-VS-28s	28	-115	66	2100	15	118.1
HDPE/MCM41-OES-7h	7	-113	54	1280	20	70.5
HDPE/MCM41-OES-7s	7	-110	53	945	19	52.4
HDPE/MCM41-OES-25s	25	-114	67	2060	16	145.5

Figure Captions

Figure 1 *^{29}Si CP/MAS NMR spectra for the different mesoporous materials analyzed: neat MCM-41; MCM-41-VS; and MCM-41-OES (from top to bottom).*

Figure 2 *Diffraction profiles at either middle (MAXS, left plot) or wide (WAXS, right plot) angles at room temperature for the HDPE homopolymer, MCM-41 and the different hybrids. Some of the MAXS patterns have been omitted and the WAXS ones have been vertically shifted for the sake of clarity.*

Figure 3 *TEM micrographs for different hybrids at similar silane functionalized MCM-41 content: HDPE/MCM41-VS-8h, HDPE/MCM41-VS-9s and HDPE/MCM41-OES-7s, from top to bottom, respectively.*

Figure 4 *DSC first melting curves for HDPE homopolymer and the hybrids, at 10 ºC/min. The inset represents an augment at the specific temperature interval.*

Figure 5 *Crystallinity values determined from: X ray profiles (f_c^{WAXS}); total DSC enthalpy during the first run; DSC enthalpy related to the main melting process; and DSC enthalpy ascribed to the confinement peak endotherm centered at around 70-80 ºC.*

Figure 6 *Thermogravimetry curves under air (left plot) and inert (right plot) environments for the different hybrids synthesized by using MCM-41 microparticles functionalized with VS (upper curves) and with OES (right curves). HDPE has been represented in all the cases for a better comparison.*

Figure 7 *Temperature dependence of the real and imaginary components of complex modulus, E', and E'' as well as of the loss tangent, tan δ, for the different samples.*

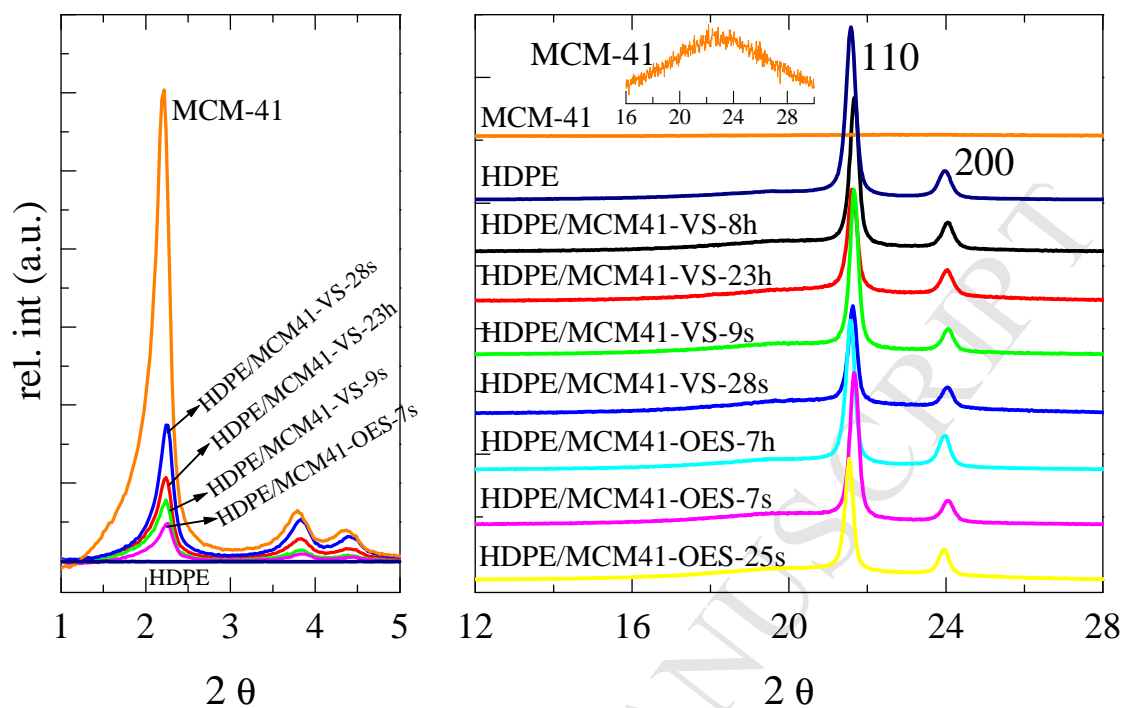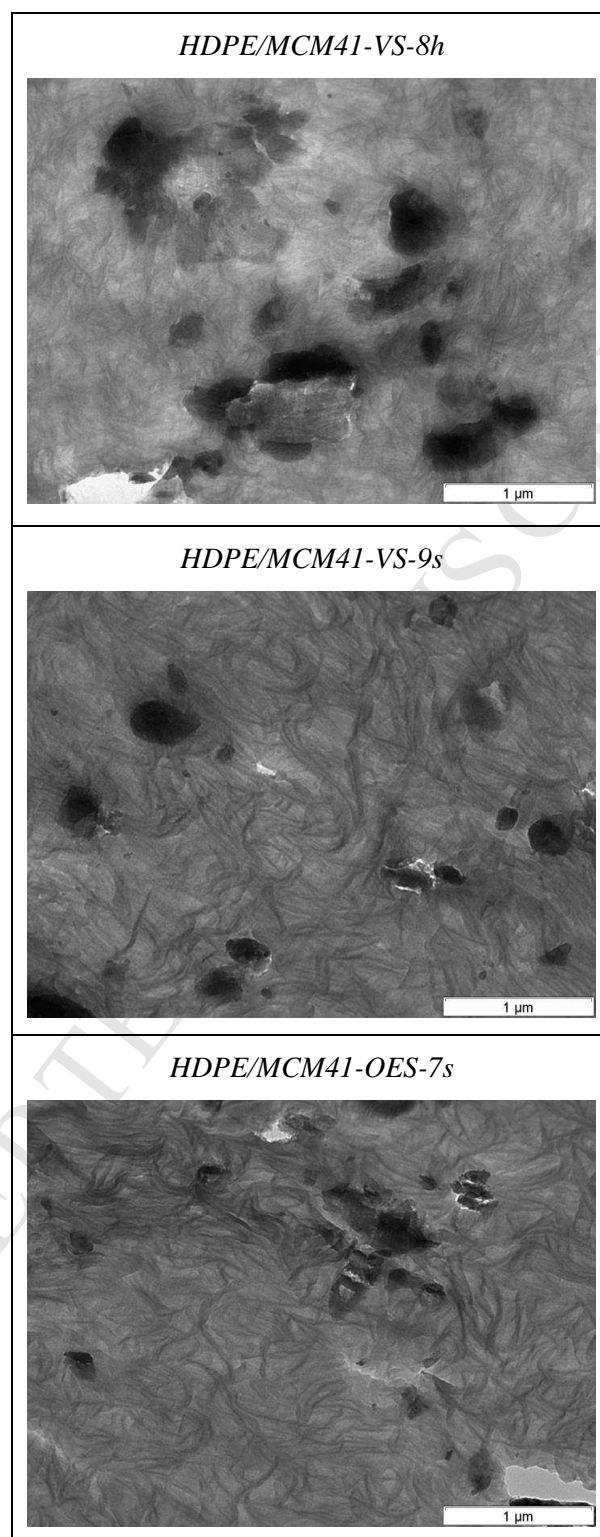Figure 8 *Load-maintenance-unload vs. depth curves for the different hybrids under study.*
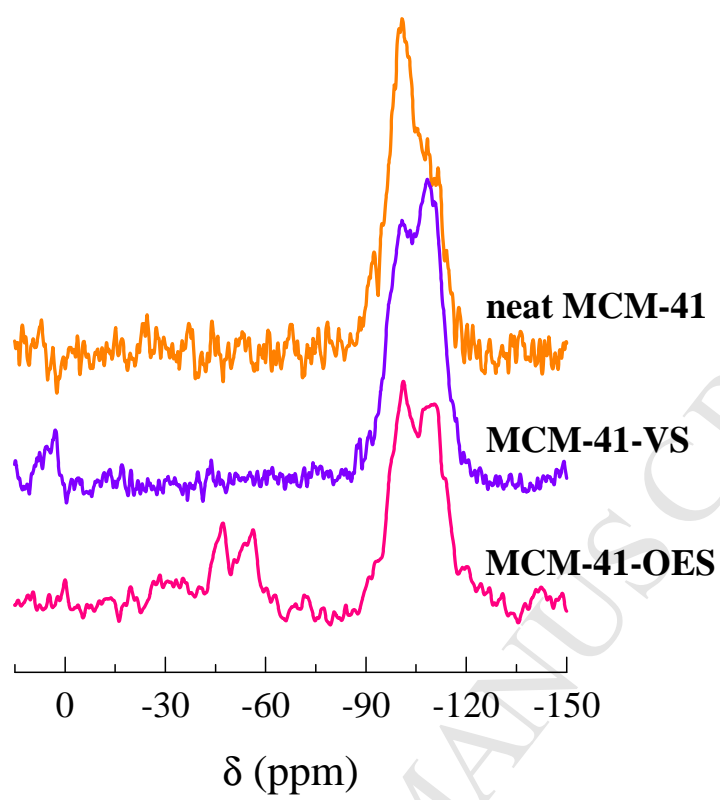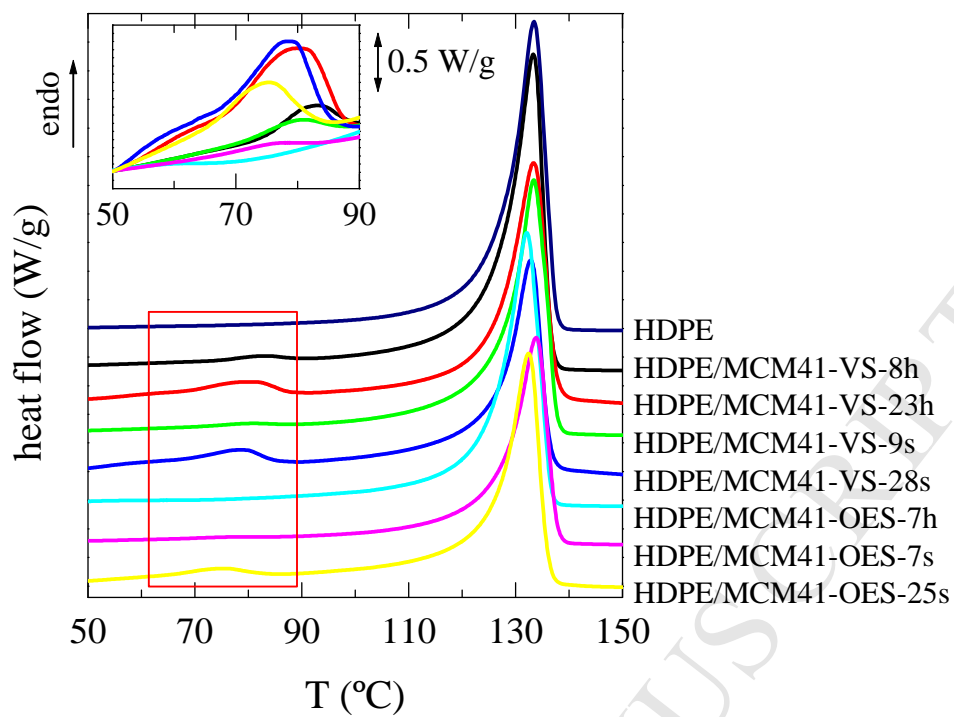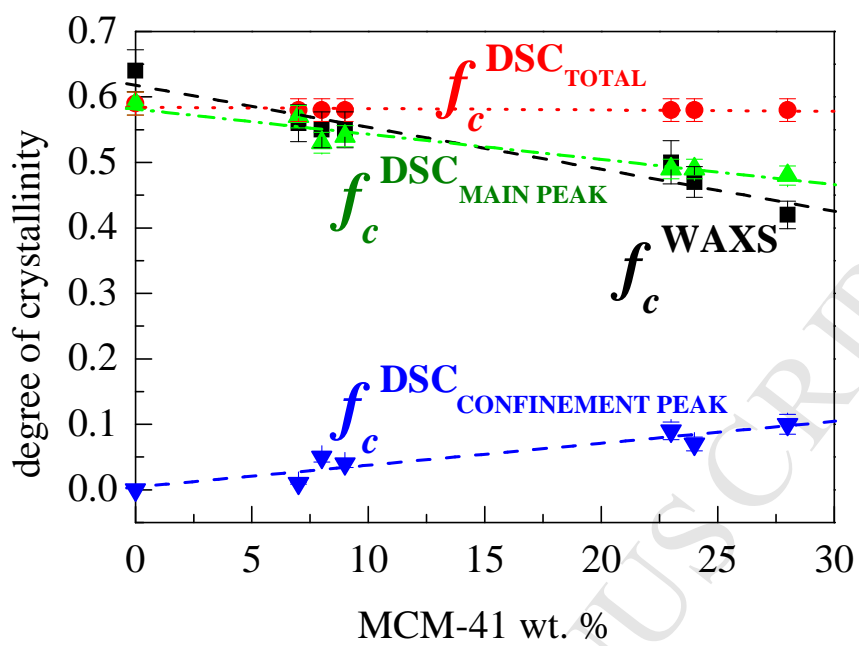
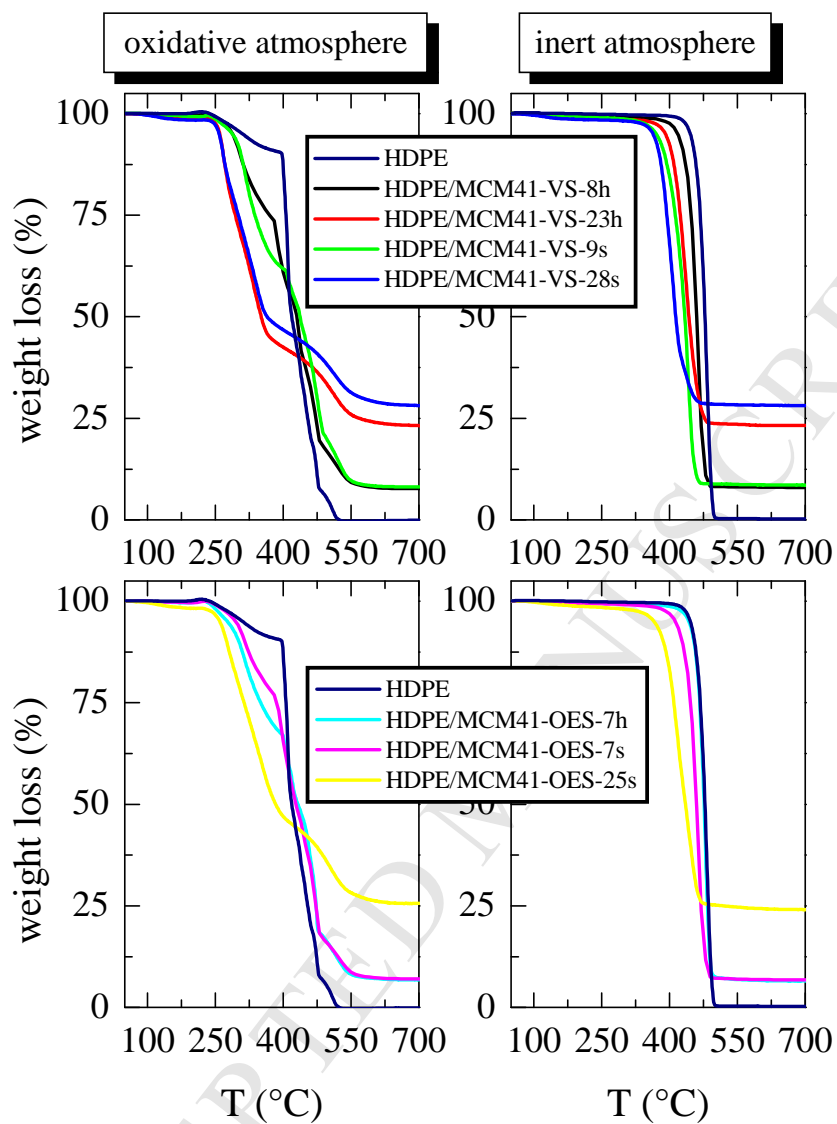*Figure 1*

Figure 2

Figure 3.
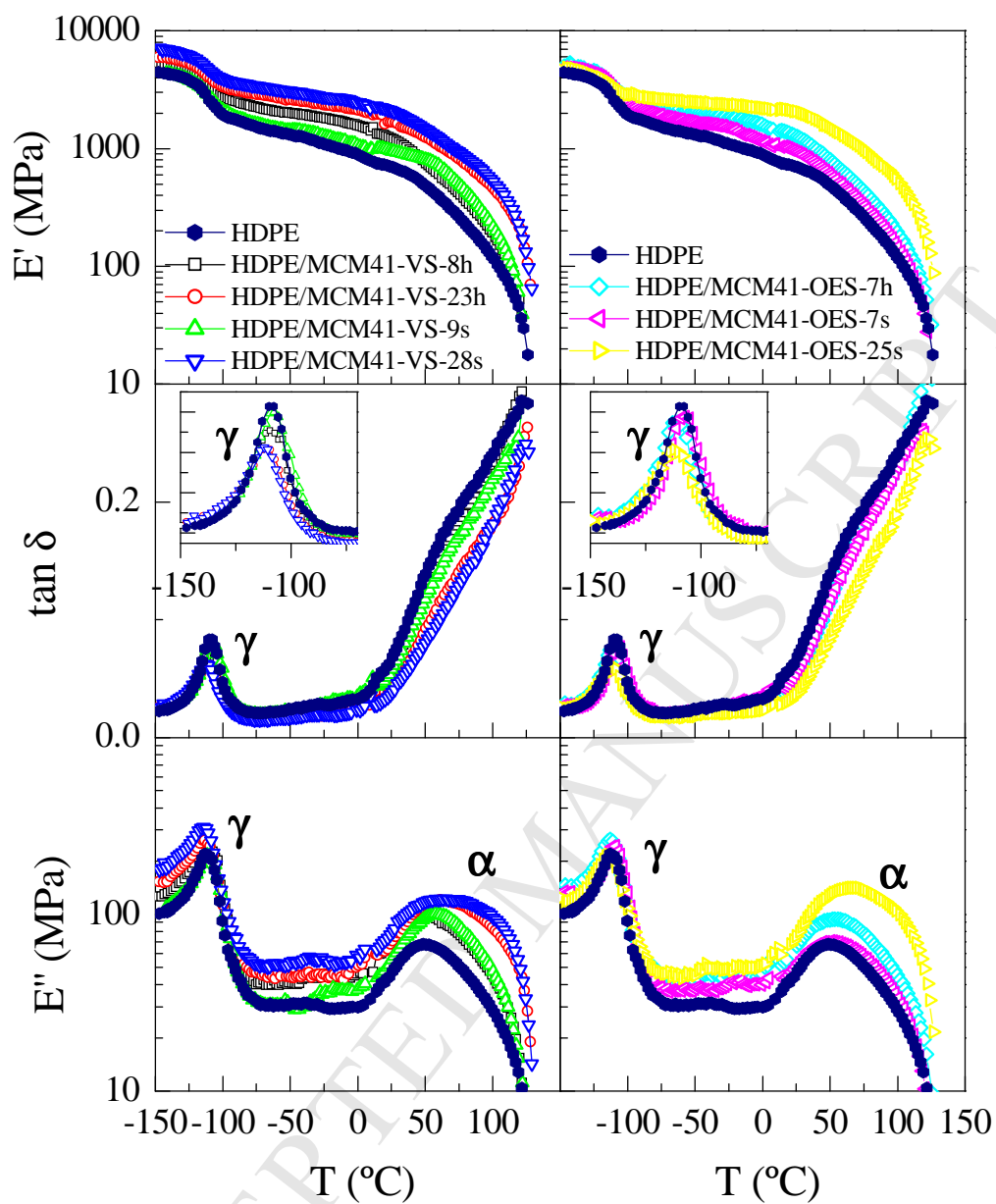
Figure 4

.

Figure 5
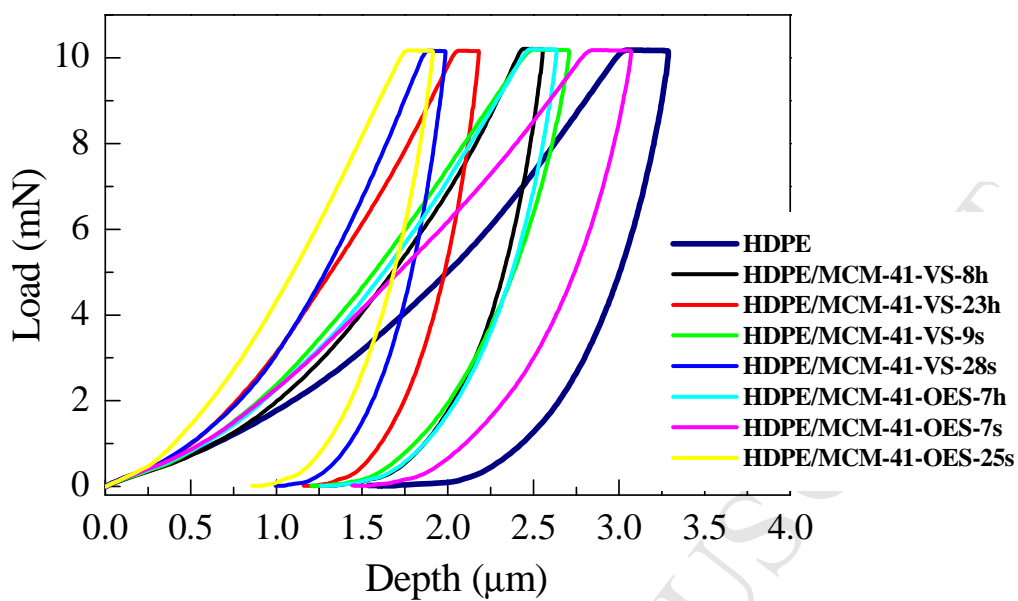
Figure 6.

Figure 7.

Figure 8.

o Materials based on polyethylene and functionalized MCM-41 particles have been synthesized

o Several approaches with silanes have been performed to decorate MCM-41 microparticles

o Changes on active species stability seem to occur from MCM-41-OES to MCM-41-VS supports

o Decorated MCM-41 particles act as catalyst carrier as well as filler.

o A secondary endothermic process appears at around 80 ºC. The resulting materials are, then, nanocomposites

o MCM-41 incorporation improves the ultimate mechanical performance without varying the final processing temperature.